THE EFFECT OF OVERLOADS UPON FATIGUE CRACK TIP OPENING DISPLACEMENT AND CRACK TIP OPENING/CLOSING LOADS IN ALUMINUM ALLOYS

James Lankford and David L. Davidson

Department of Materials Sciences, Southwest Research Institute, San Antonio, Texas, U.S.

ABSTRACT

In situ SEM observations of loaded and unloaded fatigue cracks subjected to overloads are described. Overload retardation is described phenomenologically, and crack tip opening displacements and opening/closing loads are measured. Implications of the results in terms of the effective stress intensity are discussed.

KEYWORDS

Overload; fatigue; plastic zone; crack tip opening displacement; grain boundary; opening load.

INTRODUCTION

Fatigue crack growth in aluminum alloys can be severely retarded by periodic overloads. The cyclic duration of this retardation is alloy dependent, and can vary widely (Chanani, 1977). The concepts of effective stress intensity and crack closure (Elber, 1971) have evolved in order to explain this and other load spectrum effects. Currently, there exists controversy (Macha, Corbly, and Jones, 1979; Ohta, Kosuge, and Sasaki, 1979; Lindley and Richards, 1974) as to the most appropriate way in which to measure and define crack closure, hence the effective stress intensity. The objective of this paper is to describe the results of a study of overload retardation in several aluminum alloys, using a new technique for measuring crack opening displacement and crack opening/closing loads. This direct observational approach bypasses the controversy surrounding the more indirect techniques (Lindley and Richards, 1974; Macha, Corbly, and Jones, 1979). In addition, the technique provides information regarding the physical micromechanisms involved in overload crack tip yielding and extension.

EXPERIMENTAL APPROACH

Single-edge-notched fatigue specimens with 2.5 mm thick gage sections were machined from commercial 7075, 2024, and 6061 aluminum alloys; these were then heat treated to the conditions shown in Table 1 (mechanical properties from Landgraf, 1977), polished, etched, and fatigue precracked. Overload fatigue tests were

carried out in a scanning electron microscope (SEM) using a special in-situ servo-controlled hydraulic loading stage (Davidson and Nagy, 1978). Cycling was performed at frequencies of 0.5-2 Hz, a cyclic stress intensity of $\Delta K \simeq 10$ MNm$^{-3/2}$, and a stress ratio (R) of ~0.2. Superimposed on this load spectrum were occasional spike overloads of magnitude equal to $2\Delta K$, i.e., the crack was subjected to 100% overloads (Fig. 1).

TABLE 1 Material Properties

Alloy	Yield Strength (MN/m^2)	Monotonic Strain Hardening Coefficient	Cyclic Strain Hardening Coefficient
7075-T6	470	.11	.10
2024-T4	300	.20	.09
6061-T6	290	.04	.10

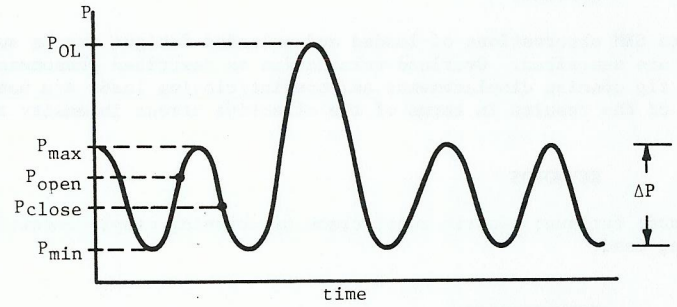

Fig. 1. Load-time sequence during overload tests.

Through this approach, crack tip yielding was monitored before, during, and after each overload, and post-overload crack growth was monitored in very small increments. Stereoimaging (Davidson, 1979) of the tips of unloaded versus (step) loaded cracks was used to accurately determine the true crack tip opening and closing loads (P_{open} and P_{close}, Fig. 1) during pre- and post-overload fatigue cycling. It should be noted that the objective in this program was to characterize some of the micromechanics involved in overload retardation; hence, a few specimens were studied in considerable detail.

RESULTS

Crack Growth Retardation

The crack growth rate results were generally similar to those that have been reported in other studies (Chanani, 1977; von Euw, Hertzberg, and Roberts, 1972), i.e., for each alloy, it was observed that during post-overload cycling, the crack experiences an initial acceleration in its rate of growth. This is followed by a period in which the crack growth decreases to some minimum value, gradually returning to the (approximate) pre-overload rate. Examples of this behavior are shown in Fig. 2, where crack growth rate da/dN is plotted versus post-overload cycles (N) for 7075-T6 and 2024-T4 aluminum. Superimposed on the crack growth

trends outlined above is a growth rate discontinuity which was observed often, and which was caused by crack tip-grain boundary interaction. For all three alloys, the pre-overload growth rate was on the order of .03-.05 μm/cycle, diminishing to .005-.01 μm/cycle at the point of maximum retardation.

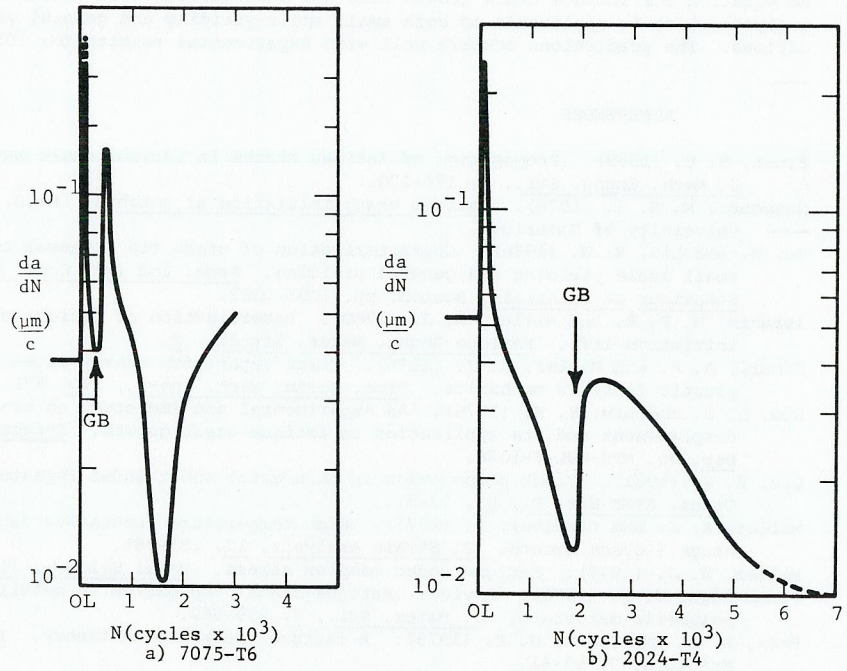

Fig. 2. Representative overload crack growth retardation.

Crack Opening and Extension

Typical crack opening sequences corresponding to the retardation exemplified above are shown in Fig. 3, for 6061-T6. Prior to the overload, at $P = P_{max}$, the crack tip is blunted and sheared open (arrow indicates shear band) to a CTOD of approximately 1.0 μm (Fig. 3a). Application of an overload (P_{OL}) produces a large crack tip opening displacement (Fig. 3b) on the order of 9.0 μm, with the blunting being accommodated in two strong slip bands oriented at approximately 70° to the plane of the crack. Upon returning to pre-overload cycling conditions, the acceleration phase of crack growth begins; this extension occurs exclusively in the heavily deformed overload shear bands. As shown in Fig. 3c, for $P = P_{max}$ at 160 cycles past the overload, the main crack has extended down the right hand shear band, and begun to change direction (arrow) in order to reorient itself normal to the load axis (Note that the overload CTOD does not relax totally; the maintaining of a residual displacement at the overload location throughout subsequent cycling was typical of all three alloys. The size of this displacement ranged from 1.0 to 2.5 μm, and was inversely proportional to the strength of the alloy.). The crack slows with further cycles, reaching its minimum growth rate, in this case, at 2,500 post-overload cycles. At this point, following approximately 94 μm of post-overload extension, the crack tip opening at $P = P_{max}$ is unmeasurable. The tip is very

sharp, and stereoimaging at magnifications as high as 4000X yields no discernible evidence of crack tip shear.

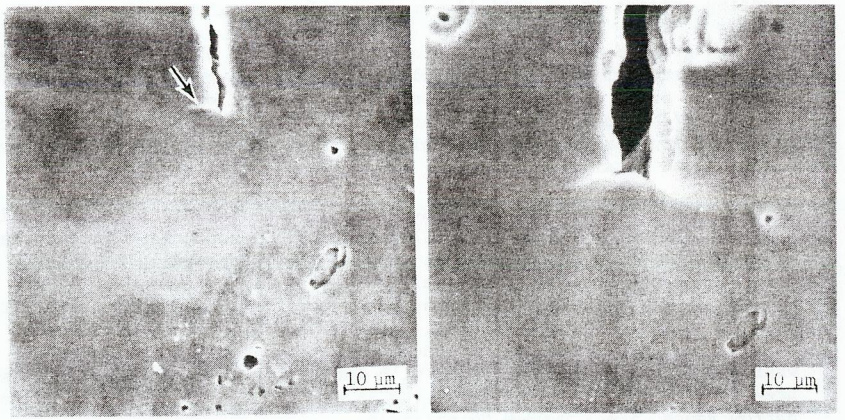

a) Pre-overload, $P = P_{max}$ b) Overload, $P = P_{OL}$

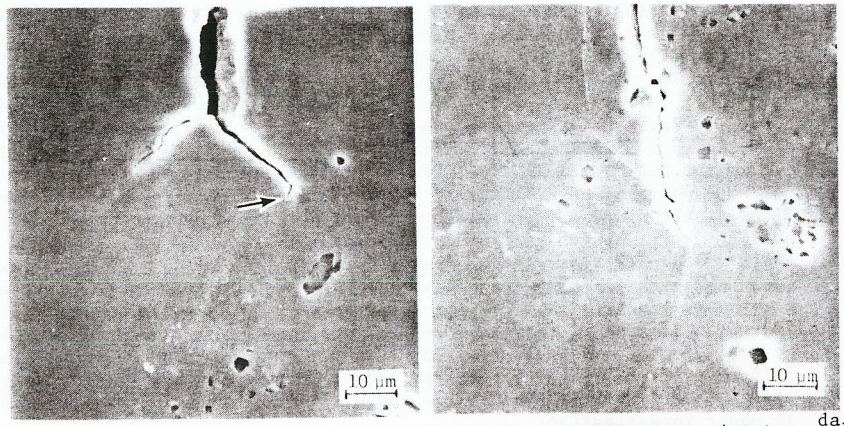

c) Overload + 160 cycles, $P = P_{max}$ d) Overload + 2500 cycles (minimum $\frac{da}{dN}$), $P = P_{max}$

Fig. 3. 6061-T6, overload sequence.

Similar behavior is shown by the other alloys; Fig. 4 represents an equivalent sequence for the 7075-T6 overload whose da/dN retardation was shown in Fig. 2a. As before, the overload occurs in two strong bands, this time oriented at ~90° and ~45° to the plane of the crack (Fig. 4a). During the transient acceleration phase, extension again occurs in one of the shear bands, in this case the one at 45° (Fig. 4b). Prior to attaining the minimum retarded growth rate, the crack encounters the grain boundary (GB) shown in Figs. 4a-c, and its rate is reduced prematurely. Upon crossing the boundary, the rate increases to that which would have corresponded solely to the position of the crack relative to the overload (Fig. 2a), finally decreasing to the overload retardation minimum at the location of the

arrow in Fig. 4c. As for the 6061-T6, at this point the CTOD is unmeasurable even for $P = P_{max}$.

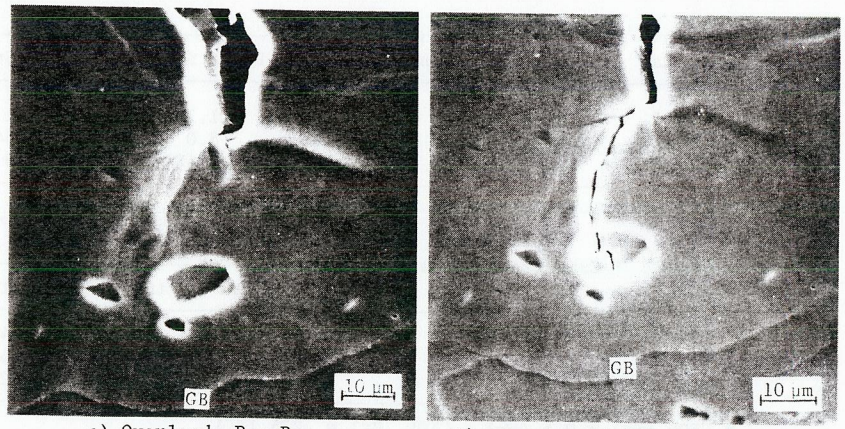

a) Overload, $P = P_{OL}$ b) Overload + 38 cycles, $P = P_{max}$

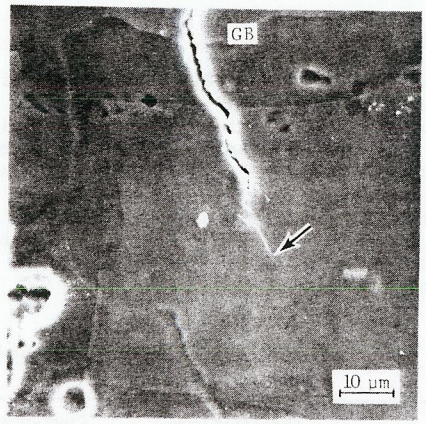

c) Overload + 1600 cycles (minimum $\frac{da}{dN}$), $P = P_{max}$

Fig. 4. 7075-T6, overload sequence.

Crack Opening Displacement

These experiments provide a rare opportunity to accurately measure crack tip opening displacements, the results of which are summarized in Table 2, and compared with theoretical estimates (Rice, 1967). The overload CTOD's show good agreement with plane stress estimates, while the pre-overload cyclic CTOD's are somewhat less than plane strain calculations would predict. In agreement with these results, the maximum cyclic stress intensity theoretically commensurate with plane strain for the weakest alloy, 6061-T6, was about 10 $MNm^{-3/2}$. Measurement of the miniscule CTOD at the minimum da/dN was not possible.

TABLE 2 Crack Tip Open Displacements

Material	Experimental Overload CTOD (μm)	Theoretical Overload CTOD* (μm)	
		Plane Stress	Plane Strain
6061-T6	10 ± 1	11.36	5.1
2024-T4	8 ± 1	8.0	3.64
7075-T6	7 ± 1	6.48	2.9

Material	Experimental Pre-Overload Cyclic CTOD (μm)	Theoretical Pre-Overload Cyclic CTOD*(μm)	
		Plane Strain	Plane Stress
6061-T6	≤0.875	1.28	2.84
2024-T4	≤0.625	0.93	2.06
7075-T6	≤0.25	0.73	1.62

* CTOD (Pσ) = 0.5 $(\frac{K}{\sigma_y})^2$; CTOD (Pε) = .225 $(\frac{K}{\sigma_y})^2$

Crack Opening Load

The effect of the residual stress field associated with the overload is clearly reflected in the crack opening and closing loads, as shown in Table 3. Results are presented in terms of the effective load ratios (Elber, 1971) U_{open} and U_{close}; the smaller the value of U, the smaller the corresponding "effective" stress intensity range $\Delta K_{eff} \equiv U\Delta K$ (Elber, 1971). Prior to an overload, U_{open} apparently decreases with alloy strength, from 0.52 for 6061-T6 to 0.37 for 7075-T6, averaging 0.44 for the three alloys. U_{close}, on the other hand, is relatively constant, averaging 0.72. Following an overload, the loads required to open a crack steadily increase, until at the minimum da/dN, U_{open} averages only 0.09, and U_{close} is approximately 0.27.

TABLE 3 Crack Tip Opening Load Ratios

Material	Pre-Overload		Post-Overload (minimum $\frac{da}{dN}$)	
	U_{open}*	U_{close}*	U_{open}*	U_{close}*
6061-T6	.52	.75	.22	.31
2024-T4	.43	.64	.03	.29
7075-T6	.37	.78	.13	.20
Average	.44	.72	.09	.27

* $U_{open} = \frac{P_{max} - P_{open}}{\Delta P}$; $U_{close} = \frac{P_{max} - P_{close}}{\Delta P}$

DISCUSSION

From the preceding results, it is possible to gain some insight as to the origin of the differences in retardation period for 2024-T4 versus 7075-T6 and 6061-T6.

First, since the experimental overload CTOD's for all three alloys can be accurately predicted by the same plane stress theory, there is no difference in the relative degree of crack tip blunting due to application of an overload. Moreover, the in situ SEM observations indicate that the basic mechanism of the blunting process is essentially identical for the three alloys.

Although grain boundary interactions were found to play a role in impeding crack extension, this is not a principal factor in crack growth retardation. This conclusion is based on the observation that the location of the crack tip at the minimum da/dN usually was not associated with a grain boundary. Rather, the site of the minimum seems to be determined by residual stress effects associated with the overload strain field.

Our results indicate that the pre-overload value for U_{open} is inversely related to alloy strength, and is generally smaller than would be expected based on the Elber relationship for 2024-T3 Al (Elber, 1971); according to which U = 0.5 + 0.4 R. The physical significance of U_{close} in crack extension is not known, but $U_{close} > U_{open}$ reflects the extensive hysteretic energy associated with forward and reverse crack tip plasticity. It is interesting that despite the systematic alloy dependent differences in the pre-overload cyclic CTOD and U_{open} results, whereby both parameters decrease with increasing yield strength, the steady-state pre-overload crack growth rates, for $\Delta K \simeq 10$ $MNm^{-3/2}$, were confined to a rather narrow range, i.e., 0.03-0.05 μm/cycle.

The post-overload U_{open} results for minimum da/dN translate into extremely low effective stress intensities; in the case of 2024-T4, for which the crack was open only the last 3% of each load half-cycle, ΔK_{eff} = 0.3 $MNm^{-3/2}$, well below the generally accepted 2024-T4 fatigue crack growth threshold. For 7075-T6 and 6061-T6, ΔK_{eff} = 1.3 and 2.2 $MNm^{-3/2}$, respectively (Fleck and Anderson, 1969). These data correspond to the (average) overload retardation periods (N_R) shown in Table 4. This table includes the retarded cycle data of Chanani (1977) for 7075-T6 and 2024-T3, since the scope of the present program does not include testing of many multiple specimens for statistical lifetime purposes. Sufficient 6061-T6 specimens have been run, however, to provide an approximate value for N_R. Clearly, the ΔK_{eff} values predicted from the true CTOD measurements correlate qualitatively with the measured retardation periods. The 7075-T6 and 6061-T6 ΔK_{eff} values are close to the respective threshold stress intensity factors, in agreement with the mild retardation found experimentally. While we hesitate to place too much significance into the monotonic strain hardening coefficients listed in Table 1, it is possible that the greater retardation shown by 2024 is at least partly due to its strain hardening capacity being greater than that of 7075 and 6061. This would be expected to induce larger residual compressive stresses in 2024 overload plastic zones, and thereby lower ΔK_{eff}. This point is under investigation.

TABLE 4 Effective Stress Intensity and Associated Crack Growth Retardation, $\Delta K = 10$ $MNm^{-3/2}$, 100% Overload

Material	K_{eff} ($MNm^{-3/2}$)	N_R ($\times 10^3$ cycles)
2024-T4	0.3	110*
7075-T6	1.3	9
6061-T6	2.2	8

*(N_R for 2024-T3)

CONCLUSIONS

1. Overload crack tip blunting is phenomenologically identical for the three alloys studied, and predictable by plane stress theory.

2. Grain boundaries act as barriers to crack growth following overloads, but do not constitute the primary source of retardation.

3. U_{open} is alloy dependent; prior to an overload, it varies inversely with strength; following an overload, it is inversely proportional to monotonic strain hardening.

4. The effect of a 100% overload is to reduce U_{open}, hence ΔK_{eff}, by 65-93%, depending on the alloy.

5. The high degree of retardation exhibited by 2024 Al in comparison with 7075 and 6061 is reflected in its sub-threshold ΔK_{eff} at the post-overload minimum crack growth rate.

ACKNOWLEDGEMENT

The authors gratefully acknowledge the support of the U.S. Air Force Office of Scientific Research, Contract No. F49620-78-C-0022.

REFERENCES

Chanani, G. R. (1977). Effect of thickness on retardation behavior of 7075 and 2024 aluminum alloys. Flaw Growth and Fracture, ASTM STP 631, American Society for Testing and Materials, Philadelphia, 365.

Davidson, D. L., and A. Nagy (1978). A low-frequency cyclic-loading stage for the SEM. J. Phys. E, 11, 207.

Davidson, D. L. (1979). Fatigue crack tip displacement observations, J. Mat. Sci., 14, 231.

Elber, W. (1971). The significance of crack closure. Damage Tolerance in Aircraft Structures, ASTM STP 486, American Society for Testing and Materials, Philadelphia, 230.

Fleck, W. G., and R. B. Anderson (1969). A mechanical model of fatigue crack propagation. Fracture 1969, 790.

Landgraf, R. W. (1977). Cyclic stress-strain responses in commercial alloys. Work Hardening and Tension in Fatigue, ed. A. W. Thompson, AIME, N.Y., 240.

Lindley, T. C., and C. E. Richards (1974). The relevance of crack closure to fatigue crack propagation. Mat. Sci. Eng., 14, 281.

Macha, D. E., D. M. Corbly, and J. W. Jones (1979). On the variation of fatigue-crack-opening load with measurement location. Exp. Mech., 19, 207.

Ohta, A., M. Kosuge, and E. Sasaki (1979). Change of fatigue crack closure level with gauge location along crack line. Int. J. Frac., 15, R53.

Rice, J. R. (1967). Mechanics of crack tip deformation and extension by fatigue. Fatigue Crack Propagation, ASTM STP 415, American Society for Testing and Materials, Philadelphia, 247.

von Euw, E. F. J., R. W. Hertzberg, and R. Roberts (1972). Delay effects in fatigue crack propagation. Stress Analysis and Growth of Cracks, ASTM STP 513, American Society for Testing and Materials, Philadelphia, 230.